Article

Induction of the Endoplasmic Reticulum Stress Pathway by Highly Cytotoxic Organoruthenium Schiff-Base Complexes

Mun Juinn Chow, Maria Babak, Kwan Wei Tan, Mei Chi Cheong, Giorgia Pastorin, Christian Gaiddon, and Wee Han Ang

Mol. Pharmaceutics, **Just Accepted Manuscript** • DOI: 10.1021/acs.molpharmaceut.8b00003 • Publication Date (Web): 06 Jul 2018

Induction of the Endoplasmic Reticulum Stress Pathway by Highly Cytotoxic Organoruthenium Schiff-Base Complexes

Mun Juinn Chow,[*,1] Maria V. Babak,[2] Kwan Wei Tan,[3] Mei Chi Cheong,[3] Giorgia Pastorin[2,4], Christian Gaiddon[5, 6] and Wee Han Ang*[*,3, 4]*

[1]Cancer Science Institute of Singapore, National University of Singapore, 14 Medical Drive, Centre for Translational Medicine, Singapore 117599

[2]Department of Pharmacy, National University of Singapore, 3 Science Drive 3, 117543 Singapore

[3]Department of Chemistry, National University of Singapore, 3 Science Drive 3, 117543 Singapore

[4]NUS Graduate School for Integrative Sciences and Engineering, Singapore

[5]U1113 INSERM, 3 Avenue Molière, Strasbourg 67200, France

[6]Oncology section, FMTS, Université de Strasbourg, Strasbourg, France

KEYWORDS

Ruthenium Arene Schiff-Base Complexes, Anticancer, p53-independent activity, Reactive Oxygen Species, Endoplasmic Reticulum Stress.

ABSTRACT

Current anticancer drug discovery efforts focus on the identification of first-in-class compounds with mode-of-action distinct from conventional DNA-targeting agents for chemotherapy. An emerging trend is the identification of endoplasmic reticulum (ER) targeting compounds that induce ER stress in cancer cells, leading to cell death. However, a limited pool of such compounds has been identified to date and there are limited studies done on such compounds to allow for the rational design of ER stress inducing agents. In our present study, we present a series of highly cytotoxic, ER stress-inducing Ru (II)-arene Schiff-Base (RAS) complexes, bearing iminoquinoline chelate ligands. We demonstrate that by structural modification to the iminoquinoline ligand, we could tune its π-acidity and influence reactive oxygen species (ROS) induction, switching between a ROS-mediated ER stress pathway activation and one that is not mediated by ROS induction. Our current study adds to the available ER stress inducers and shows how structural tuning could be used as a means to modulate the mode-of-action of such compounds.

INTRODUCTION

Conventional anti-proliferative agents target nuclear DNA leading to DNA damage that trigger concomitant activation of p53 and downstream apoptosis factors to signal for apoptotic cell death. However, phenomenon such as p53 mutation and apoptosis resistance in many cancer types has led to the decreased effectiveness of such therapeutic agents.[1-4] In cancers such as melanoma, glioblastoma and non-small cell lung cancer (NSCLC), dysregulation of the apoptosis pathway is the key mechanism responsible for resistance to chemotherapeutic treatments.[5-7] As such, p53 mutation and BAX/Bcl-2 expression serve as prognostic biomarkers for several cancer types, and p53 mutation and dysregulation of apoptotic factors such as BAX/Bcl-2 are often associated with poorer clinical outcomes from conventional chemotherapy.[8-10] Consequently, current drug discovery efforts focus on divergent strategies such as the identification and development of anticancer agents that target other cell organelles and act *via* atypical mode-of-action to circumvent the multidrug resistance phenomenon brought about by defects in the apoptotic pathway.[11-13]

One emerging trend is the identification of drug candidates that target the endoplasmic reticulum (ER) with the goal of inducing ER stress and leading to eventual cell death.[14-16] FDA-approved drugs such as Nelfinavir, Sorafenib and gold-based Auranofin are ER stress-inducing agents currently investigated and repurposed for cancer treatment.[17-21] Other novel metal-based ER stress inducers are also being investigated as anticancer drugs (Figure 1).[22-25] The recent surge in interest could be due to the implication of reactive oxygen species (ROS)-mediated ER stress in several novel strategies for cancer treatment. For instance, ROS-mediated ER stress is required to trigger Type-II immunogenic cell death, a concurrent cancer cell killing and activation of the immune system, which has been shown to significantly reduce cancer recurrence in *in vivo* models.[26-27] ER stress is also implicated in apoptosis-independent programmed cell death such as autophagy,

paraptosis and necroptosis, which could be exploited in the treatment of apoptosis-resistant cancers.[28-31] Nevertheless, the discovery of such compounds are rarely reported and there have been few structural-tuning studies performed on ER stress-inducing compounds that allow for a targeted design approach.

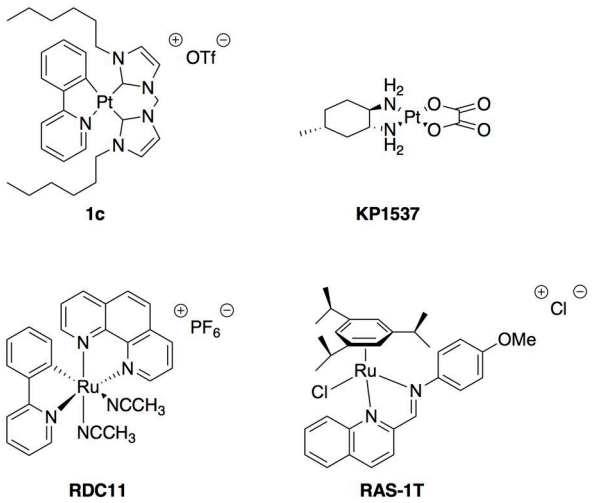

Figure 1. Cytotoxic metal complexes that induce ER stress in cancer.

We earlier identified lead anticancer complex **RAS-1T** from a class of Ru-arene Schiff-base (RAS) complexes (Figure 1).[32-34] **1** (RAS-1T) is able to induce non-apoptotic cell death in colorectal and gastric cancers through ROS-mediated ER stress. In addition, we also showed that minor structural modification to the facially-bound arene ligand on **1** could significantly affect its mode-of-action, switching from a ROS-dependent to a ROS-independent ER stress pathway.[34] Building on previous studies, we further explored how structural modification could affect the mode-of-action of this class of complexes by incorporating chelating iminoquinoline ligands of varying degrees of π-acidity. Our study showed that these 2nd generation RAS complexes had nanomolar cytotoxicity in a panel of drug-sensitive and -resistant ovarian, gastric and colorectal cancer cell lines. In addition, we demonstrate that by modifying the structural moiety on the

iminoquinoline ligand, we could tune its π-acidity and influence ROS induction, switching between a ROS-mediated ER stress pathway activation and one that is not mediated by ROS induction. Given the potential application of ER stress-inducing anticancer compounds for the treatment of resistant cancer types, our study adds to the limited pool of such compounds and provide additional information on how structural modification could be used to modulate their mode-of-action.

EXPERIMENTAL

Materials. All experimental procedures were carried out without additional precautions to exclude air or moisture unless otherwise specified. All chemicals and solvents were used as received unless otherwise specified. Dry ethanol and methanol were obtained by drying in molecular sieves 3-4 Å 24 h before use. $RuCl_3.xH_2O$ was purchased from Precious Metals Online. [(η^6-1,3,5-triisopropylbenzene)$RuCl_2$]$_2$ were synthesized according to previously reported protocols.[32] Thiazolyl blue tetrazolium bromide (MTT), IGEPAL CA-630, DL-Dithiothreitol, Tetramethylethylenediamine (TEMED), Sodium Deoxycholate, *N*-acetylcysteine, Non-fat Dried Milk Bovine, Bovine Serum Albumin, TWEEN® 20, Ponceau S and Thioredoxin Reductase Assay Kit were purchased from Sigma-Aldrich. Nitric acid (65% to 71%, TraceSELECT Ultra) was obtained from Fluka (Sigma Aldrich). Tris was purchased from Vivantis Technologies. 10% SDS solution were purchased from Life Technologies. Glycine, Hyclone™ Trypsin Protease 2.5% (10X) solution, RPMI 1640, DMEM medium, Fetal bovine serum (FBS), Hank's Balanced Salt Solution (HBSS) and Pierce™ Protease and Phosphatase Inhibitor Mini Tablets were purchased from Thermo Fisher Scientific. Hyclone™ Dulbecco's Phosphate-Buffered Saline (10x) and

Penicillin-Streptomycin (10 000 U/mL) were purchased from Ge Healthcare Life Sciences. Bio-rad Protein Assay Dye Reagent Concentrate, 30% Acrylamide/Bis solution, 4x Laemmli Sample Buffer, Nitrocellulose Membrane, 0.2 μm and 0.45 μm were purchased from Bio-rad Laboratories. Luminata™ Classico and Crescendo Western HRP Substrate were purchased from Merck Millipore Corporation. All other chemicals used were purchased from Sigma-Aldrich (Singapore). All new compounds synthesized were shown to be > 95% pure either by RP-HPLC or elemental analysis.

Instrumentation. ^{1}H NMR spectrums were obtained using a Bruker Avance 500 spectrometer and the chemical shifts (δ) were reported in parts per million with reference to residual solvent peaks. Electrospray-ionization Mass Spectrometry (ESI-MS) spectra were obtained using Thermo Finnigan MAT ESI-MS System. UV-vis spectra were obtained using the Shimadzu UV-1800 UV Spectrophotometer. Cellular Ru content was determined by Agilent 7700 Series ICP-MS (Agilent Technologies, Santa Clara, CA, USA). Ru drug stock concentrations were determined using Optima ICP-OES (Perkin-Elmer) operated by CMMAC, NUS. Elemental analyses of selected Ru complexes were carried out using a Perkin-Elmer PE 2400 elemental analyzer by CMMAS, NUS. Absorbance on 96-well plates were measured using BioTek® Synergy H1 Hybrid Reader. Western blot proteins bands were visualized *via* enhanced chemiluminescence imaging (PXi, Syngene). Flowcytometry experiments were done with BD LSRFortessa Cell Analyzer. Ultrapure water was purified by a Milli-Q UV purification system (Sartorius Stedim Biotech SA).

HPLC analysis of compound purity. Determination of the purity of **2** and **3** were done using analytical HPLC on a Shimadzu Prominence System equipped with a DGU-20A$_3$ Degasser, two LC-20AD Liquid Chromatography Pump, a SPD-20A UV/Vis Detector and a Shim Pack GVP-ODS 2.0 mm C18 column (5 μM, 120Å, 250 mm x 4.60 mm i.d.) at r.t. at a flow rate of 1.0 mL/min

with detection at both 214 nm and 254 nm. The gradient elution conditions were as follows: 20-80% solvent B over 30 min, where solvent A is 10 mM aqueous NH_4OAc pH 7.0 and solvent B is CH_3CN.

Synthesis of RAS-1T (1). Complex **1** was synthesized according to published procedure.[32]

Synthesis of 2, 3 and 4. A similar protocol was used for the syntheis of **2**, **3** and **4**. 2-Quinolinecarboxaldehyde (59.0 mg, 0.375 mmol), and 4-ethylaniline (46.5 µl, 0.375 mmol) or *N,N*-dimethyl-*p*-phenylenediamine (51.1 mg, 0.375 mmol) or 4-isopropylaniline (51.3 µl, 0.375 mmol) was added to dry EtOH (5 mL) and and stirred at r.t. over 24 h. The solvent was removed *in vacuo* and the resultant crude products were redissolved in MeOH (15 mL). Subsequently, $[(\eta^6$-1,3,5-triisopropylbenzene)$RuCl_2]_2$ (127 mg, 0.169 mmol) was added and stirred at r.t. over 12 h. The solvent was removed *in vacuo* and the resulting solid purified by column chromatography (1:4 v/v EtOH/$CHCl_3$, R_f = 0.5-0.6). The final products were then dried *in vacuo* for 1 h to give a final product.

2: Red-brown solid. Yield: 66 mg (31%). ^{1}H NMR (500 MHz, DMSO-d6): δ 9.13 (s, 1H), 8.95 (d, J = 9 Hz, 1H), 8.87 (d, J = 9 Hz, 1H), 8.3 (m, 2H), 8.13 (t, J = 8 Hz, 1H), 8.04 (d, J = 8 Hz, 2H), 7.98 (t, J = 8 Hz, 1H), 7.48 (d, J = 8 Hz, 2H), 5.57 (s, 3H), 2.75 (q, J = 8 Hz, 2H), 2.41 (sept, J = 7 Hz, 3H), 1.26 (t, J = 8 Hz, 3H), 1.15 (d, J = 7 Hz, 9H), 0.84 (d, J = 7 Hz, 9H) ppm. ESI-MS (+ve mode): m/z = 601 $[M]^+$. Purity of the complex was determined to be >95% pure by RP-HPLC and elemental analysis. RP-HPLC (% Purity): 96.5% at 214 nm and 95.8% at 254 nm; t_r = 30.4 min. Analysis (Calcd., found for $C_{33}H_{40}N_2Cl_2Ru.3.5H_2O$): C (56.65, 56.75), H (6.77, 6.66), N (4.00, 4.06).

3: Dark purple solid. Yield: 134 mg (62%). ^{1}H NMR (500 MHz, DMSO-d6): δ 9.00 (s, 1H), 8.95 (d, *J* = 9 Hz, 1H), 8.77 (d, *J* = 9 Hz, 1H), 8.19 (m, 2H), 8.05 (m, 2H), 7.92 (t, *J* = 8 Hz, 1H), 6.87 (d, *J* = 9 Hz, 2H), 5.49 (s, 3H), 3.09 (s, 6H), 2.50 (m, 3H), 1.17 (d, *J* = 7 Hz, 9H), 0.86 (d, *J* = 7 Hz, 9H) ppm. ESI-MS (+ve mode): m/z = 616 $[M]^+$. Purity of the complex was determined to be >95% pure by RP-HPLC (% Purity): 97.4% at 214 nm and 97.0% at 254 nm; t_r = 28.5 min.

4: Red-brown solid. Yield: 108 mg (49%). ^{1}H NMR (500 MHz, DMSO-d6): δ 9.14 (s, 1H), 8.94 (d, *J* = 9 Hz, 1H), 8.87 (d, *J* = 9 Hz, 1H), 8.29 (m, 2H), 8.14 (t, *J* = 7 Hz, 1H), 8.03 (d, *J* = 9 Hz, 2H), 7.99 (t, *J* = 8 Hz, 1H), 7.51 (d, *J* = 8 Hz, 2H), 5.58 (s, 3H), 3.05 (sept, *J* = 7 Hz, 1H), 2.39 (sept, *J* = 7 Hz, 3H), 1.29 (dd, *J* = 7 Hz, 6H), 1.15 (d, *J* = 7 Hz, 9H), 0.85 (d, *J* = 7 Hz, 9H) ppm. ESI-MS (+ve mode): m/z = 615 $[M]^+$. Purity of the complex was determined to be >95% pure by elemental analysis. Analysis (Calcd., found for $C_{34}H_{42}N_2Cl_2Ru.2.5H_2O$): C (58.70, 58.55), H (6.81, 6.67), N (4.03, 4.12).

UV-vis analysis of compound stability. 1 – 4 were dissolved at a final concentration of 50 μM in 1.5 ml of ddH_2O, DMSO, aqueous NAC (2 mM) or DMEM containing 10% FBS (without phenol red). The UV-vis profiles of the samples were monitor by UV-vis over 24 h at 1h-intervals.

Determination of Log P. Log P_{ow} of **2**, **3** and **4** were determined using the shake flask method.[35] The RAS complex were dissolved in ddH_2O that was presaturated with *n*-octanol (for 24 h and left to stand until phase separation occurs). The UV-vis spectrum for each samples was obtained and the absorbances at the λ_{max} of each compound were determined. Equal volume of *n*-octanol was added to each sample solution and the heterogeneous mixtures shaken for 2 h before centrifuging at 4000 rpm for 1 min to achieve phase separation. The final absorbance of the aqueous phase at

the λ_{max} of each compound were determined and their water-octanol partition coefficient were calculated. All experiments were done in triplicate.

Tissue culture. The human colorectal carcinoma cells HCT116 and HCT116 $p53^{-/-}$ pair were gifts from Professor Shen Han-ming (NUS). Human gastric adenocarcinoma AGS and Human colorectal adenocarcinoma HT29, were acquired from ATCC® (Manassa, VA). Human ovarian carcinoma cells A2780 and A2780cisR were obtained as gifts from Professor Paul Dyson (EPFL). TC7 cells were cloned from parental colorectal adenocarcinoma Caco-2 cells by the limited dilution technique.[36] HT29, HCT116 and HCT116 $p53^{-/-}$ cells were cultured in DMEM medium containing 10% FBS and 1% Penicillin/Streptomycin. A2780, A2780cisR and AGS cells were cultured in RPMI 1640 medium containing 10% FBS and 1% Penicillin/Streptomycin. TC7 cells were cultured in DMEM medium containing 20% FBS, 1% Penicillin/Streptomycin and 1% NEAA. All cell lines were grown at 37 °C in a humidified atmosphere of 95% air and 5% CO_2. Experiments were performed on cells within 20 passages.

Inhibition of cell viability assay. The anti-proliferative activity the RAS Complexes on exponentially growing cancer cells were determined using MTT assay as described previously.[37] HT29, AGS, HCT116, HCT116 $p53^{-/-}$ and TC7 were seeded at 5 000 cells per well (100 µL), and A2780 and A2780cisR were seeded at 6000 cells and 10 000 cells per well (100 µL) respectively in Corning® Costar® 96-well plates and incubated for 24 h. Thereafter, cancer cells were exposed to drugs at different concentration in media for 48 h. The final concentration of DMSO in medium was < 1% (v/v) at which cell viability was not significantly inhibited. The medium was removed and replaced with MTT solution (100 µL, 0.5 mg/mL) in media and incubated for an additional 45 min. Subsequently, the medium was aspirated, and the purple formazan crystals dissolved in DMSO (100 µL). The absorbance due to the dissolved purple formazan was then obtained at 570

nm. Inhibition to cell viability was evaluated with reference to the IC_{50} value, which is defined as the concentration needed for a 50% reduction of survival based on the survival curves. IC_{50} values were calculated from the dose - response curves (cell viability vs drug concentration) obtained in repeated experiments and adjusted to actual [Ru] administered, which was determined using ICP-OES. The experiments were performed in 3 replicates for each drug concentration and were carried out at least three times independently.

For cell viability assays involving ROS quencher, NAC (2 mM) was added at the same time and co-incubated with drugs for the entire 48 h duration. Cell viability in the absence and presence of NAC was normalized against untreated control. Experiments were performed in 3 replicates and carried out at least three times independently.

ROS detection. HCT116 cells were harvested by trypsinization and 1 mL of cell solution (2×10^5 cells per ml) was centrifuged (5 min, 2500 rpm) and washed with 1 mL of HBSS and centrifuged again (5 min, 2500 rpm). The supernatant was replaced with 20 μM of 2′,7′-dichlorodihydrofluorescein diacetate (H_2DCFDA) in HBSS and the cells were incubated for 10 min at 37 °C in the absence of light for probe activation. The cells were then centrifuged (5 min, 2500 rpm) and the supernatant was replaced with the drug solutions in colorless DMEM without FBS at desired concentrations. The cells were then incubated with drug solutions for 4 h at 37 °C in the absence of light. After 4 h, the cell solutions were immediately strained with a 60 μM cell strainer prior to analysis by flow cytometry. 0.46 g/L propidium iodide (PI) was added to the strained samples to identify the dead cells. Trolox (100 μM) was used as ROS scavenger in the control sample. The data was processed and exported using BD FACSDiva 6.2 and the quantity of ROS species was normalized to untreated control stained with H_2DCFDA probe only. Evaluation was based on the mean of at least three independent experiments.

Cellular uptake of Ru. HCT116 cells were seeded into Cellstar 6-well plates (Greiner Bio-one) at a density of 400 000 cells/well. After the cells were allowed to resume exponential growth for 24 h, they were exposed to **1 – 4** at their respective IC50 values for 24 h. The cells were washed twice with 1 ml of PBS and lysed with lysis buffer [100 µL, 1% IGEPAL CA-630, 150 mM NaCl, 50 mM Tris-HCl (pH 8.0)] for 5–10 min at 4 °C. The cell lysates were scraped from the wells and transferred to separate 1.5 mL microtubes. The supernatant was then collected after centrifugation (13 000 rpm, 4 °C for 15 min) and total protein content of each sample was quantified via Bradford's assay. Cell lysates were transferred to 2 ml glass vials and then digested with ultrapure 65% HNO_3 at 100˚C for 24 h. The resulting solution was diluted to 2-4% v/v HNO_3 with ddH_2O water. Ru content of each sample was quantified by ICP-MS using Re as an internal standard. Ru and Re were measured at m/z 101 and m/z 186, respectively. Metal standards for calibration curve (0, 0.5, 1, 2, 5, 10, 20, 40 ppb) were freshly prepared before each measurement. Ru and Re standards for ICP-MS measurements were obtained from CPI international (Amsterdam, The Netherlands). All readings were made in triplicates in He mode.

Thioredoxin Reductase Inhibition Assay. Assays were performed according to the protocol provided by manufacturer. Briefly, 180 µl of working buffer [100 mM pH 7.0 potassium phosphate, 10 mM EDTA and 0.24 mM NADPH], 8 µl of 1x assay buffer [100 mM pH 7.0 potassium phosphate and 10 mM EDTA], 2 µl of Enzyme solution (10 ng) was added to each well of a Corning® clear 96-well plate. 4 µl of complexes **1 – 4** was added to the appropriate wells to give a final concentration of 1x or 2x [IC_{50}]. The reaction mixture was incubated with gentle shaking at room temperature for 30 min. Subsequently, 6 µl of DTNB (100 mM) was added and incubated for an additional 3 mins. Thereafter, the absorbance at 412 nm were measured every minute for the next 30 min. A separate set of positive control experiments were performed using

the inhibitor provided with the kit. % enzyme activity was calculated from the data obtained with reference to control sample without inhibitor.

Antibodies and Western blot protocol. HCT116 cells were grown at 500 000 cells per well (2 mL) on Corning® Costar® 6-well plates for 24 h before being treated with **1** - **4** at IC_{50} or IC_{75} for 6 h and 24 h. OXP was used as a positive control at the same effective concentrations. For experiments involving ROS quencher, NAC (2mM) was added at the same time and co-incubated for the entire duration. Subsequently, the cells were lysed with RIPA lysis buffer [100 µL, 0.1% SDS, 0.5% Sodium Deoxycholate, 1% IGEPAL® CA-630, 150 mM NaCl, 25 mM Tris-HCl (pH 8.0), protease and phosphatase inhibitor cocktail]. The cell lysates were transferred to separate 1.5 mL tubes and sonicated for 3 x 15 s. The samples were then centrifuged at 13000 rpm, 4˚C for 15 min. The liquid supernatant containing the proteins were collected and total protein content of each sample was quantified *via* Bradford's assay. 50 µg of proteins from each sample were reconstituted in loading buffer [100 mM DTT, 1x Protein Loading Dye] and heated at 95˚C for 5 min. The protein mixtures were resolved on 10% SDS-PAGE gel by electrophoresis and transferred to a 0.2 µm nitrocellulose membrane. Protein bands were visualized *via* enhanced chemiluminescence imaging (PXi, Syngene) after treatment with the appropriate primary and HRP-conjugated secondary antibodies. Equal loading of protein was confirmed by comparison with actin expression. The following antibodies were used: p53 (FL-393) (sc-6243) and p21 (F-5) (sc-6246) from Santa Cruz Biotechnologies. CHOP (D46F1), PERK (D11A8), IRE1α (14C10) and phospho-eif2α from Cell Signaling Technologies. β-Actin (ab8229) from Abcam. Pierce™ HRP-conjugated anti-rabbit IgG (H+L) (#31460), anti-mouse IgG (H+L) (#31430) and anti-goat IgG (H+L) (#31402) from Thermo Fisher Scientific. All antibodies were used at 1:1000 dilutions except for actin (1:10000), anti-mouse, anti-goat and anti-rabbit (1:5000).

RESULTS & DISCUSSION

Design consideration, synthesis and characterization

In our previous work, we identified structural motifs common to the library of p53-independent RAS complexes with diverse physico-chemical properties that were important for the high efficacy and p53-independent anticancer activity, namely the triisopropylbenzene (TPB) arene moiety and the quinoline ligand.[33] In the present study, using **1** as the core structure, we perform minor structural modification to the iminoquinoline chelate ligand to modulate its π-acidity (Figure 2). This was done by replacing the **4-OMe** (**1**) moiety with more electron-donating **4-NMe$_2$** (**3**) (less π-acidic) or with their corresponding isoelectronic counterparts, namely **4-Et** (**2**) and **4-iPr** (**4**), which do not contain any conjugated lone-pair electrons (more π-acidic). We performed structural tuning studies on these new complexes alongside **1** to study how the changes in chelate ligand π-acidity could affect properties such as p53-dependence, ROS and ER stress-induction.

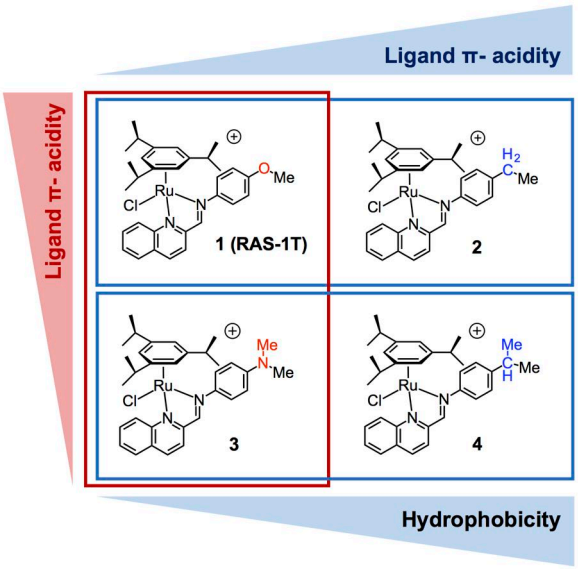

Figure 2. RAS complexes investigated in the present study. Hydrophobicity and π-acidity of the chelating ligands were modulated by varying the highlighted functional moiety.

New complexes **2 – 4** were synthesized using a similar protocol for the synthesis of **1** (Scheme 1).[32] Briefly, 2-quinolinecarboxyaldehyde and aniline derivatives, containing either the **4-NMe$_2$**, **4-Et** or **4-iPr** moiety, were added to dry EtOH and allowed to react at r.t. to give the iminoquinoline ligands with varying degrees of purity. The crude ligands were used directly for chelation with stoichiometric amount of the TPB-Ru precursor in MeOH to give the corresponding RAS complex, after purification by silica gel column as crystalline solids. Their identities were verified by ^{1}H NMR and ESI-MS analysis and their purities were determined to be >95% by RP-HPLC or elemental analysis. The ^{1}H NMR of **2 – 4** showed resonances typical of RAS complexes.[32-34] The signal corresponding to the imine proton at ca. 9.1 ppm, and the additional splitting pattern of the TPB protons signals indicated the formation and chelation of the iminoquinoline to the Ru center (Supplementary Information (SI), Figure S1, S3 and S5). Their ESI-MS spectra showed only the characteristic $[M]^+$ ion with Ru and Cl isotopic pattern (SI, Figure S2, S4 and S6) and tandem MS-MS gave expected fragmentation patterns.

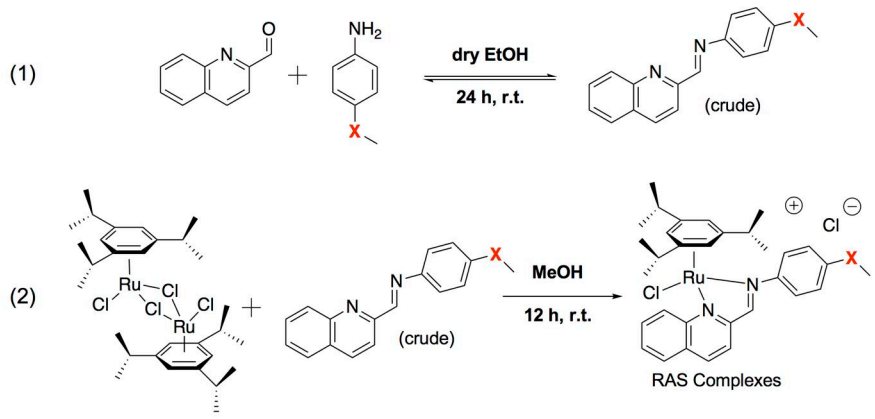

RAS Complexes	X =	
1	-O-	(4-OMe)
2	-C-H$_2$	(4-Et)
3	-N-Me	(4-NMe$_2$)
4	H-C-Me	(4-iPr)

Scheme 1. General synthetic route for 2nd Generation RAS complexes.

Influence of Schiff-base ligands functional moiety on π-acidity and stability

We studied how the structural modifications and chelate ligand π-acidity affected physiochemical properties such as stability and hydrophobicity, which are important factors that influence RAS complexes' biological activity. We first confirmed the order of chelate ligand π-acidity by comparing the UV-vis spectrums and λ_{max} of the RAS complexes. In principle, the lower the π-acidity of the ligand (less π-backbonding) the higher the energy of the Ru π-HOMO, which would result in a smaller π - π* (HOMO-LUMO) energy gap. This means that a lower excitation energy (higher λ_{max}) would be required for a π - π* transition in a complex with a less π-acidic ligand. Indeed, complexes containing motif with conjugated lone-pair electrons such as **1** and **3** exhibited λ_{max} at 387 nm and 460 nm, respectively, validating the lower π-acidity of their chelate ligand (Figure 3). Conversely, complexes having more π-acidic ligands without conjugated lone-pair electrons, such as **2** and **4**, exhibited much lower λ_{max} at 365 nm. Therefore, the degree of iminoquinoline ligand π-acidity was established to be **2** ≈ **4** > **1** > **3**, in agreement to our initial design considerations and theoretical predictions.

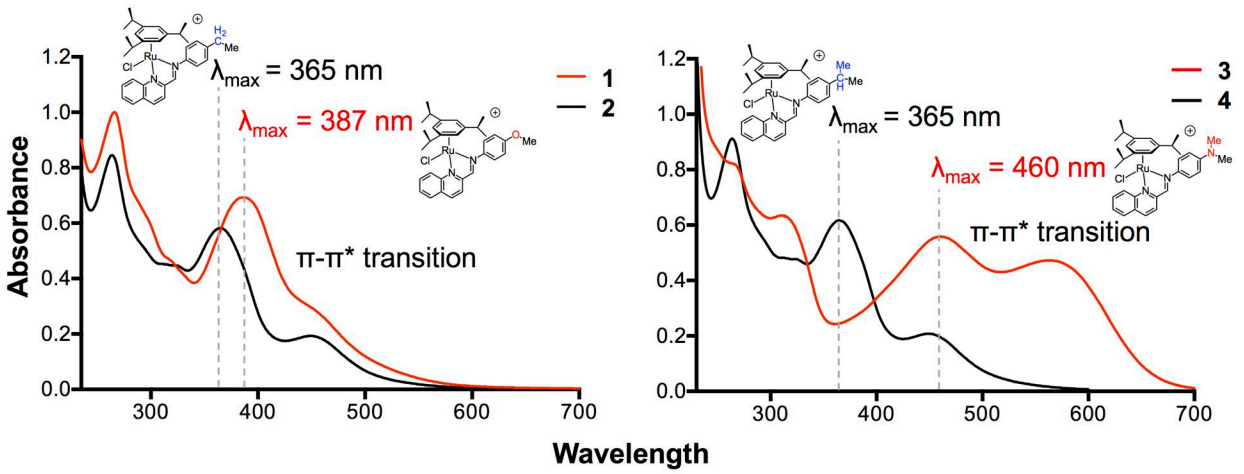

Figure 3. UV-vis spectrum confirms the ranking order of chelate ligand π-acidity. Lower π-acidity of the chelate ligand results in lower energy π-π* transition as indicated by a higher λ_{max}. Therefore, the order of chelate ligand π-acidity: **2** ≈ **4** > **1** > **3**.

Next, we determined the stability of the RAS complexes in different media such as double-distilled water (ddH_2O), Dulbecco's Modified Eagle's Medium (DMEM) with 10% fetal bovine serum (FBS), and aqueous *N*-acetylcysteine (NAC, 2 mM) by monitoring their UV-vis profile over 24 h. Any chemical interactions between the complexes and the media leading to the formation of new chemical species would manifest in a gradual shift in the UV-vis profile over time. All RAS complexes demonstrated stability towards hydrolysis in ddH_2O (SI, Figure S7). In DMEM with 10% FBS, **3** having the least π-acidic chelate ligand exhibited minimal changes in UV-vis profile, demonstrating the greatest stability (Figure 4a). This was consistent with our previous study showing that a less π-acidic ligand results in the more electron-rich Ru center, stabilizing the Ru-Cl bond and making it more resistant to substitution by 'N'- or 'S'- containing nucleophiles.[33] In keeping with these observations, **1** was previously shown to be stable in Hank's Balanced Salt Solution (HBSS) buffer containing 10% FBS and aqueous solutions of biological nucleophiles such as glutathione and dGMP.[32, 34] Its instability in DMEM with 10% FBS suggest that reaction with the Ru-Cl bond is still possible in medium containing high concentration of nucleophiles (DMEM is modified from Basal Medium Eagle (BME) and contains 4x more amino acids and vitamins. It also has 4.5x more glucose than HBSS). It is noteworthy that the trend in stability was reversed in aqueous NAC. RAS complexes **1**, **2** and **4** had unchanged UV-vis profile after 24 h in NAC while a significant shift was observed for **3** (Figure 4b). Since **3** demonstrated the greatest stability towards substitution reaction, we postulated that the shift in UV-vis profile was likely due to a redox reaction between the electron-rich Ru center of **3** and the reducing NAC. However, more studies would be required to fully understand the interaction between NAC and **3**.

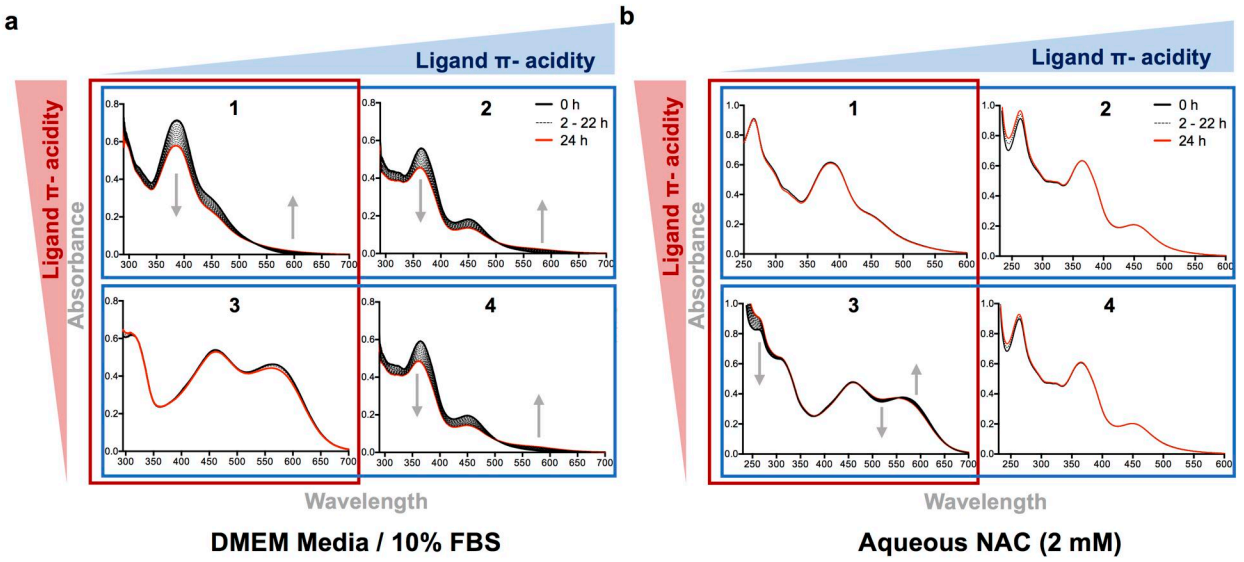

Figure 4. π-acidity of the chelating ligands affects the stability of the RAS complexes to nucleophilic substitution or reduction. UV-vis profile of RAS complexes in (a) DMEM media with 10% FBS and (b) aqueous NAC (2 mM). Grey arrows indicate regions of increasing or decreasing absorbance over time.

The log P_{OW} of **1 – 4** were determined by the shake-flask method using UV-vis spectroscopy analysis.[35] In general, log P_{OW} of the RAS complexes followed an expected trend and structural modification from the core RAS-1T structure such as addition of methyl groups (**4-Et → 4-iPr**) or replacing hydrogen-bonding heteroatoms (N, O) with isoelectronic CH_x groups (**4-OMe → 4-Et; 4-NMe_2 → 4-iPr**) had a predictable effect in log P_{OW} (Table 1; SI, Figure S8). All compounds had log P_{ow} in the negative range, in keeping with previous studies.[33] This was presumably due to the charged nature of the RAS complexes containing neutral chelate ligands.

Efficacy studies in drug-sensitive and –resistant cancers and p53-independent studies

To ascertain the anti-proliferative activity of **1 – 4,** we tested them against of a panel of drug-sensitive and -resistant cancer cell lines that include ovarian (A2780, A2780cisR), gastric (AGS) and colorectal (HT29, HCT116, HCT116 $p53^{-/-}$, TC7) cancers, and measured cell viability 48 h

after treatment using standard MTT assay. We included cisplatin (CDDP), oxaliplatin (OXP) and 5-fluorouracil (5-FU) as clinical drug controls and compare the efficacies of the RAS complexes to these controls, particularly in cancer lineages that are drug-resistant. For example, ovarian A2780cisR is a CDDP-resistant variant of A2780 wild-type and its resistance arises from the accumulation of mutated p53 and more efficient DNA repair mechanism.[38-39] p53-null colorectal HCT116 $p53^{-/-}$ is less sensitive to p53-dependent anticancer agents such as OXP and 5-FU compared to its wild type lineage.[40] Lastly, the multidrug-resistant TC7 demonstrated low sensitivity towards most apoptosis-inducing drugs such as OXP, 5-FU and doxorubicin in a panel of colorectal cancer cell lines,[34, 41] due to numerous defects in its apoptotic machinery, such as its $p53^{-/0}$ status and increased expression of anti-apoptotic Bcl-2/Bcl-x_L.[41] Compounds efficacious against these cell lines would have a greater potential in the treatment of multidrug-resistant cancers.

Table 1. Cytotoxicity data for second generation RAS Complexes.

Complex	Log P_{ow}[a]	IC_{50} [μM] [b]						
		A2780	A2780cisR	AGS	HT29	HCT116 wt	HCT116 $p53^{-/-}$	TC7
1 (RAS-1T)	-0.85 ± 0.02	0.53 ± 0.15	0.87 ± 0.22	0.74 ± 0.14	0.91 ± 0.07	1.14 ± 0.12	0.73 ± 0.12	2.95 ± 0.18
2	-0.62 ± 0.01	0.37 ± 0.09	0.49 ± 0.08	0.54 ± 0.04	0.42 ± 0.04	0.53 ± 0.11	0.39 ± 0.11	1.37 ± 0.07
3	-0.55 ± 0.01	0.29 ± 0.06	0.43 ± 0.09	0.38 ± 0.06	0.39 ± 0.03	0.46 ± 0.05	0.27 ± 0.05	1.60 ± 0.12
4	-0.31± 0.03	0.35 ± 0.12	0.46 ± 0.04	0.45 ± 0.04	0.38 ± 0.05	0.47 ± 0.05	0.34 ± 0.05	1.02 ± 0.04
Oxaliplatin	n.d.	n.d.	n.d.	n.d.	1.16 ± 0.08	3.23 ± 0.81	16.7 ± 5.4	15.1 ± 4.1
5-Fluorouracil	n.d.	n.d.	n.d.	n.d.	5.88 ± 1.95	7.33 ± 2.25	33.6 ± 17.4	396 ± 133
Cisplatin	n.d.	1.36 ± 0.11	7.73 ± 1.08	29.3 ± 2.1	n.d.	n.d.	n.d.	n.d.

[a]Log P_{ow} values determined via the shake-flake method against 1:1 *n*-octanol:H_2O partitioning. [b]IC_{50} values is the concentration of Ru complexes required to inhibit 50% of cell growth with respect to control groups, measured by MTT assay after 48 h of incubation. Data obtained are based on the average of three independent experiments, and the reported errors are the corresponding standard deviations. The IC_{50} were corrected using actual [Ru] determined using ICP-OES.

Compound **1 – 4** displayed nanomolar IC_{50} values in both drug-sensitive cell lines (A2780, AGS, HT29, HCT116) and drug-resistant phenotypes (A2780cisR, HCT116 $p53^{-/-}$); in multidrug-resistant TC7, **1 – 4** displayed low micromolar IC_{50} values (Table 1). In all cell lines, **1 – 4** were several times more efficacious than clinical drugs CDDP, OXP and 5-FU. This was most apparent when comparing their activities in the drug-resistant cell lineages. For instance, **1 – 4** had resistance factor between 1.3 – 1.6 in A2780cisR/A2780 pair while CDDP showed resistant factor of 5.7 (Table 2; SI, Figure S9a). In HCT116 $p53^{-/-}$/HCT116 cell pair, **1 – 4** had p53-dependence factor < 1 while OXP and 5-FU had much higher values of 5.2 and 4.6 respectively (Figure 5a, Table 2). Lastly, **1 – 4** demonstrated apoptosis-resistance factor between 2.2 – 3.5 in TC7/HCT116 cell pair while OXP and 5-FU displayed higher resistance factor of 4.6 and 54 respectively (Table 2; SI, Figure S9b). Taken together, **1 – 4** showed high efficacies against both drug-sensitive and drug-resistant cell phenotypes and were much less affected by the same resistance mechanisms impeding the activities of clinical drugs such as CDDP, OXP and 5-FU in A2780cisR, HCT116 $p53^{-/-}$ and TC7 cells.

Table 2. Resistance factor for RAS Complexes.

Complex	Resistance Factor[a]	p53-Dependence Factor[b]	Apoptosis Resistance Factor[c]
	Ratio of IC_{50} (A2780cisR / A2780)	Ratio of IC_{50} (HCT116 $p53^{-/-}$ / HCT116)	Ratio of IC_{50} (TC7/HCT116)
1 (RAS-1T)	1.6	0.6	2.6
2	1.3	0.7	2.6
3	1.5	0.6	3.5
4	1.3	0.7	2.2
Oxaliplatin	n.d.	5.2	4.7
5-Fluorouracil	n.d.	4.6	54
Cisplatin	5.7	n.d.	n.d.

[a, b, c] Resistance Factors were calculated by taking the ratio of IC_{50} in resistant cell lines and sensitive cell line; a smaller value represents a greater selectivity towards resistant cell lines.

We further confirmed the p53-independent activity of **1 – 4** by investigating the induction of p53 and downstream target p21 in HCT116 cells after drug treatment (Figure 5b), in comparison with OXP as the positive control. In general, **1 – 4** showed a lack of induction of p53 regardless of concentration or duration of treatment. A slight induction of p21 was observed with **1**, **2** and **3** only after 24 h exposure at IC_{75} concentration, likely *via* p53-independent pathways.[42] In contrast, p53-dependent OXP induced a strong upregulation of both p53 and p21 in a concentration and time-dependent manner.

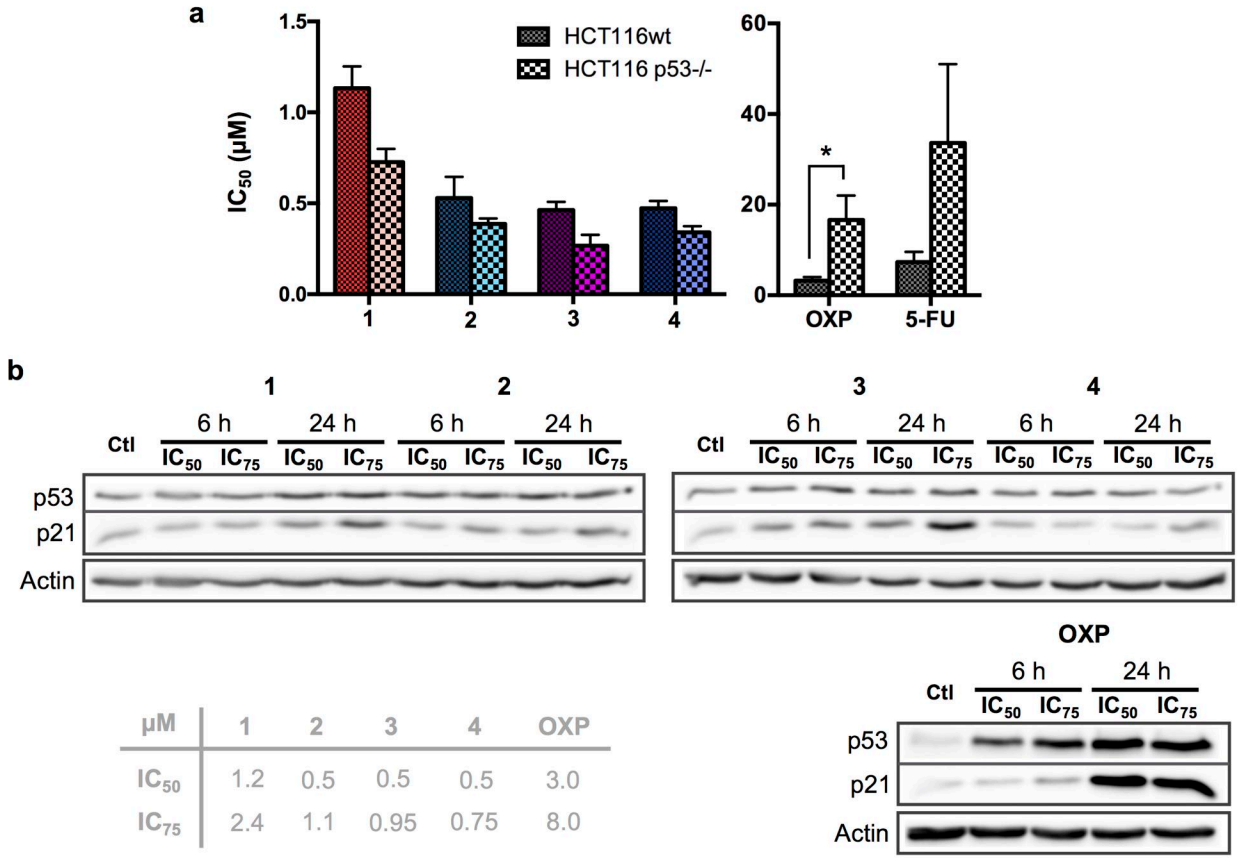

μM	1	2	3	4	OXP
IC_{50}	1.2	0.5	0.5	0.5	3.0
IC_{75}	2.4	1.1	0.95	0.75	8.0

Figure 5. RAS Complexes display p53-independent activity. (a) IC_{50} values of RAS complexes, oxaliplatin and 5-fluorouracil after 48h treatment in both HCT116wt and HCT116 $p53^{-/-}$ cells. Mean ± s.e.m. (* $p < 0.05$; two-tailed Student's t-test). (b) Western blot analysis of p53 and target p21 in HCT116 cells after treatment with RAS complexes and oxaliplatin at IC_{50} and IC_{75} for 6h and 24h. Homogeneous protein loading determined with reference to actin.

Tuning π-acidity of chelate ligand allows modulation of ROS-induction

Many metallodrugs including **1** has been shown to induce ROS leading to cell death, due to the redox active nature of metal complexes.[43] However, there are limited study on how the electron-donating/accepting ability of ligands affect ROS induction by these metal complexes. Hence, we investigate if varying the ligand π-acidity in the present series of compounds affects cellular ROS accumulation.

Cellular ROS was quantified using flow cytometry after cell staining with commercially available, cell-permeable ROS probe, H_2DCFDA. HCT116 cells were pre-stained with H_2DCFDA before treatment with varying concentrations of **1 – 4** for 4 hours. Thereafter, the treated samples were analyzed and compared to the stained, untreated control. Compounds **1**, **2** and **4** induced ROS in a concentration-dependent manner (Figure 6). **2** and **4** having the most π-acidic ligands, were the strongest ROS inducers, increasing cellular ROS by 2.6-fold and 3.5-fold at 5 μM treatment while ROS induction by **1** was more modest only achieving 2.5-fold at a higher concentration of 15 μM. In contrast, **3** having the least π-acidic ligands, only increased ROS levels modestly when treated at the highest concentration of 15 μM with no increase in ROS at treatment concentration less than 10 μM. The results suggested a strong correlation between degree of chelate ligand π-acidity and ROS induction, following the order **2** ≈ **4** > **1** > **3**. It is also noteworthy that complexes with less stable Ru-Cl bonds demonstrated stronger ROS induction. It is possible that a certain degree of Ru-Cl bond lability was required for the RAS complexes to participate directly with cellular redox reactions, disrupting redox homeostasis and resulting in the accumulation of ROS.[43]

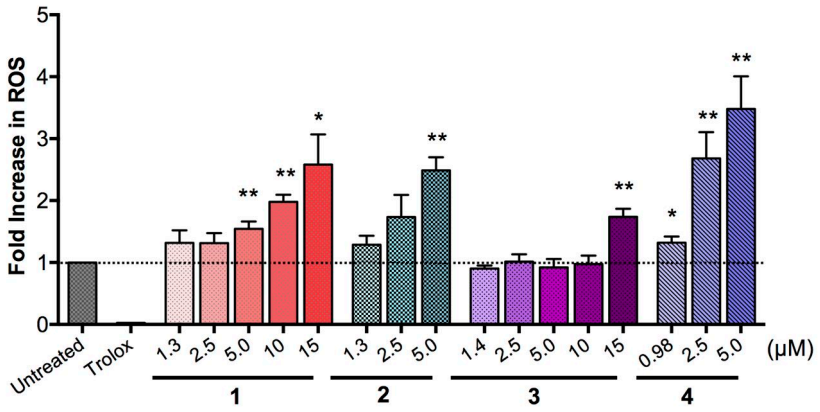

Figure 6. Chelate Ligand π-acidity influences degree of ROS-induction. Detection of ROS with H_2DCFDA (20 μM) after treatment with RAS complexes for 4 h using flow cytometry measurements. Mean ± s.e.m. (* $p < 0.05$, ** $p < 0.01$; Student's t test).

To ascertain if the degree of cellular accumulation affects ROS-induction, we quantify Ru content in the cell after drug treatment by ICP-MS analysis. Briefly, HCT116 cells were treated with compounds **1 – 4** at IC_{50} concentrations for 24 h before being detached from the cell culture vessels, washed with PBS buffer and digested in 65% nitric acid with heating at 100˚C. Once the sample has dried up, the remaining residue was reconstituted and diluted in ddH_2O before Ru content in cells was quantified by ICP-MS. Compounds **1 – 4** accumulated in cells to similar extent with no significant differences ($p > 0.05$) when treated at their respective IC50 values (SI, Figure S10). Hence, any observed difference in ROS induction is not due to to differential uptake.

As there have been several reports of metal complexes causing increased cellular ROS accumulation as a direct consequence of thioredoxin reductase (TrxR) inhibition,[44-46] we investigate if this was the case for our series of complexes. We measured the percentage inhibition of mammalian TrxR by compound **1 – 4** using a colorimetric thioredoxin reductase inhibition assay according to the protocol provided by the manufacturer. All compounds did not significantly inhibit TrxR at 1x or 2x IC_{50} concentrations, in the micromolar range (SI, Figure S11). This was

in contrast to Au complexes which has been known to inhibit TrxR at low nanomolar range.[45] Hence, we concluded that cellular ROS accumulation caused by the RAS complexes was not due to TrxR inhibition.

ROS functions as signaling molecules in many complex cellular pathways and dysregulation in any number of these pathways could result in an accumulation of ROS in the cell. Hence, identifying the exact pathway(s) implicated in ROS-induction by **1 – 4** would require more extensive studies.

Tuning π-acidity of chelate ligand affects duration and intensity of ER stress

Next, we investigated how tuning π-acidity would influence ER stress induction by **1 – 4.** Induction of ER stress would lead to the unfolded protein response (UPR), which mediates recovery, cellular dysfunction and cell death.[47] Three distinct UPR signaling pathways have been identified, namely the PERK, IRE1α and ATF6 pathway.[48] We focused our investigation on two of the three UPR pathway, namely the PERK and IRE1α pathway by studying their accumulation and phosphorylation pattern. In addition, we probed the cellular expression of transcription factor CHOP, a common and highly-induced downstream biomarker of UPR during ER stress.[49]

Cellular IRE1α, phopho-IRE1α, PERK, phospho-PERK, p-eif2α and CHOP levels were ascertained by Western blot analysis, after treatment with **1 – 4** under various conditions. All four compounds seem to induced ER stress *via* IRE1α pathway as seen by phosphorylation of IRE1α either after 6h or 24 h treatment at IC_{75} concentration (Figure 7). Phosphorylation of IRE1α by **4** is the least intense, with only a slight induction after 6 h treatment. The lack of phosphorylation of PERK or downstream eif2α suggest that the PERK arm of the UPR pathway is not activated by treatment with **1 – 4** (SI, Figure S12). In addition, all four compounds induced concentration-

dependent upregulation of CHOP at 6 h (Figure 7). However, ER stress was more sustained for compounds with less π-acidic ligands, **1** and **3**, as seen by the significant upregulation of CHOP even at 24 h after treatment. In contrast, compounds with more π-acidic ligands, **2** and **4**, a less sustained ER stress was observed with significantly lower expression of CHOP at 24h after treatment.

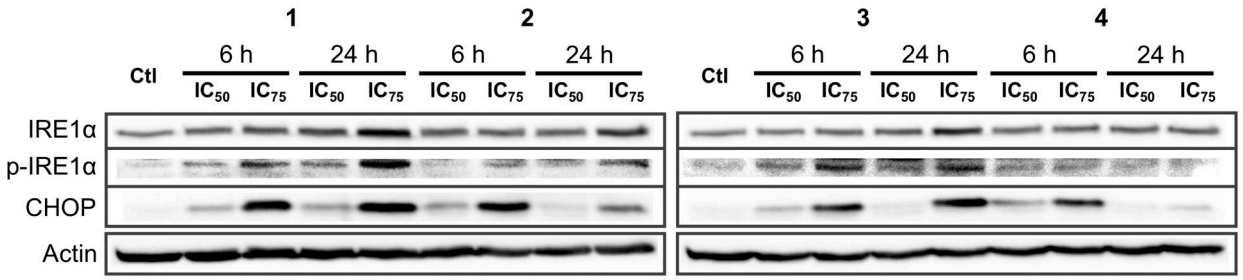

μM	1	2	3	4
LD (IC_{50})	1.2	0.5	0.5	0.5
HD (IC_{75})	2.4	1.1	0.95	0.75

Figure 7. RAS complexes induce ER stress, activating the IRE1α UPR pathway. Western blot analysis of various ER stress biomarker after 6 h and 24 h treatment with **1 – 4** at IC_{50} and IC_{75} concentrations. Homogeneous protein loading determined with reference to actin.

ROS-mediated versus ROS-independent ER stress induction

Complex **1** was previously shown to induce ROS at early time points resulting in ROS-mediated ER stress, which could be abolished by co-treatment with a ROS-quencher NAC.[34] Thus, we investigated how co-treatment with NAC influenced cell viability and ER stress induction by analogous **1 – 4**. This was done by measuring cell viability and CHOP expression in HCT116 cells after treatment with compounds **1 – 4**, in the absence and presence of NAC. For compound **1**, **2** and **4**, quenching ROS with NAC (2 mM) resulted in an almost complete protection of the cells at all treatment concentrations (Figure 8a), showing the cellular ROS accumulation was important for the activity of **1**, **2** and **4**. For compound **3**, co-incubation with NAC also provided a cyto-

protective effect to a lesser degree. However, the lack of ROS induction by **3** even at highly cytotoxic concentrations (Fig 6) suggested that ROS was not critical for its activity. Hence, the observed cyto-protective effect could be due to a 'detoxification' by the direct redox reaction between NAC and **3** (Figure 4b). Nevertheless, the exact nature of the reaction between NAC and **3** is something that requires more extensive investigation.

Based on cellular CHOP levels, NAC significantly reduced its expression in cells co-treated with **1**, **2** and **4**, suggesting that NAC could protect cells against these compounds, restoring ER homeostasis and shutting off UPR signaling (Figure 8b). In contrast, NAC had a lesser effect on CHOP expression in cells co-treated with **3**, suggesting that NAC was unable to restore ER homeostasis as effectively in this instance. This further confirmed the non-oxidative nature of the ER stress induced by **3**.

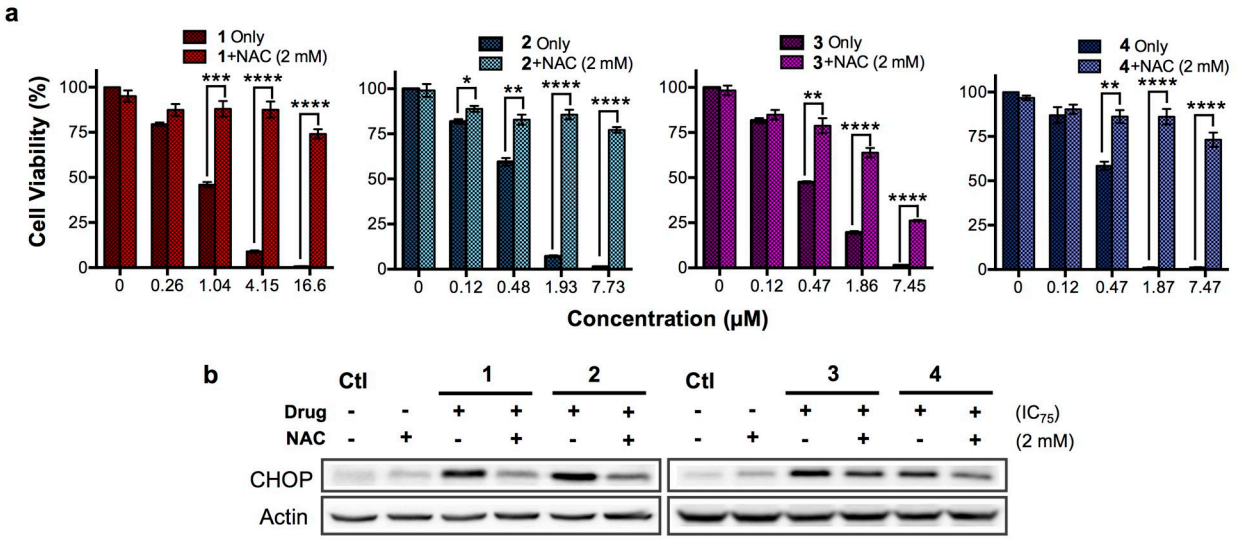

Figure 8. Tuning chelate ligand π-acidity causes a switch between ROS-mediated ER stress and ER stress not mediated by ROS induction. (a) Cell viability of HCT116 cells treated with RAS complexes after 48h treatment in the absence or presence of NAC (2 mM). Mean ± s.e.m. (* $p < 0.05$, ** $p < 0.01$, *** $p < 0.001$, **** $p < 0.0001$; two-tailed Student's t-test). (b) Western blot analysis of CHOP in HCT116 cells after treatment with RAS complexes at IC_{75} for 6h, in the absence or presence of NAC (2 mM). Homogeneous protein loading determined with reference to actin.

Taken together, the results indicated that **1**, **2** and **4** exerted their mode-of-action *via* ROS-mediated ER stress while **3** induced ER stress without corresponding ROS induction; ROS and ER stress induction were important for the activity of **1**, **2** and **4** and co-treatment with NAC restored redox and ER homeostasis and rescued cells from cell death. In contrast, **3** did not increase ROS levels and co-treatment with NAC did not mediate cell death or ER stress to the same extent. We surmised that direct tuning of the iminoquinoline ligand's π-acidity could be used a means to modulate ROS induction of RAS complexes, thereby switching from a ROS-mediated ER stress mode-of-action to an ER stress pathway that is not mediated by ROS.

CONCLUSION

We presented a new class of Ru-based ER stress inducers with high efficacies in a panel drug-sensitive and -resistant cancer types and performed structural tuning studies by varying the chelate ligand π-acidity and studying its effect on stability, ROS and ER stress induction. Our studies showed that by varying the chelate ligand π-acidity, the stability of the complexes towards substitution and redox reaction could be chemically tuned; RAS complexes containing greater chelate ligand π-acidity (**1, 2** and **4**) had more labile Ru-Cl bond that undergo substitution while RAS complex with lower π-acidic ligand (**3**) had more stable Ru-Cl but was more susceptible to redox reaction with reductant NAC due to its more electron-rich Ru center. Also, decreasing chelate ligand π-acidity on the RAS complexes reduced ROS induction and caused a switch from a ROS-mediated ER stress pathway to an ER stress pathway not mediated by ROS. This current work adds to the available pool of ER stress inducer and lends a greater understanding on how structural changes on RAS complexes affect ROS and ER stress pathway activation, which could

lead to better design of ER stress inducers with specific mode-of-action and efficacy against drug-resistant cancer types.

AUTHOR INFORMATION

Corresponding Authors*

[1]Email: csicmj@nus.edu.sg

[3]E-mail: chmawh@nus.edu.sg, Phone: +65 6516 5131.

Author Contributions

M.J.C. conceived the study, designed all experiments, performed chemical synthesis and *in vitro* experiments, and analyzed all data. M.V.B. and M.C.C. performed cellular ROS accumulation analysis. M.V.B. performed Ru cellular accumulation studies, TrxR inhibition assay and analysis, and western blot experiments. K.W.T. performed cell viability assays. C.G. and G.P advised on biological experiments. W.H.A. conceived and directed the study. M.J.C, M.V.B and W.H.A wrote the manuscript with contributions from all authors. All authors have read, edited and given approval to the final version of the manuscript.

Funding Sources

Financial support from Ministry of Education and the National University of Singapore (R143-000-638-112) and Ligue contre le cancer, CNRS, European COST action CM1105 is gratefully acknowledged.

ACKNOWLEDGEMENTS

The authors thank staff of CMMAC, NUS for performing elemental analysis and ICP-OES analysis, Paul J. Dyson (EPFL) and Han-Ming Shen (NUS) for their gift of cell lines.

ABBREVIATIONS

ROS, reactive oxygen species; ER, endoplasmic reticulum; CDDP, cisplatin; OXP, oxaliplatin, 5-FU, 5-fluorouracil; H_2DCFDA, 2′,7′-dichlorodihydrofluorescein diacetate; TrxR, thioredoxin reductase; EDTA, ethylenediaminetetraacetic acid; NEAA, non-essential amino acids; FBS, fetal bovine serum; DMEM, Dulbecco's Modified Eagle's Medium; BME, Basal Medium Eagle; NMR, nuclear magnetic resonance; ESI-MS, electrospray ionization-mass spectrometry; RP-HPLC, reverse phase-high performance liquid chromatography; DMSO-d^6, deuterated dimethyl sulfoxide; MeOH-d^4, deuterated methanol; ddH_2O, ultrapure water; ICP-OES, inductively couple plasma-optical emission spectrometry; ICP-MS, inductively couple plasma-mass spectrometry NAC, *N*-acetylcysteine; NADPH, Nicotinamide adenine dinucleotide phosphate, DTNB, 5,5-dithio-bis-(2-nitrobenzoic acid); UPR, unfolded protein response; RAS, ruthenium (II) arene Schiff-base; TPB, triisopropylbenzene; Bcl-2, B-cell lymphoma 2; Bcl-x_L, B-cell lymphoma extra large; BAX, bcl-2-associated X protein; CHOP, CCAAT-enhancer-binding protein homologous protein; PERK, PKR-like ER kinase; IRE1α, inositol-requiring enzyme 1A; ATF6, activating transcription factor 6; eif2α, eukaryotic translation initiation factor 2A; Hank's Balanced Salt Solution (HBSS); dGMP, 2′-deoxyguanosine 5′-monophosphate sodium salt hydrate.

Supporting Information Available: ^{1}H NMR, ESI-MS and UV-Vis spectrums of compounds. Thioredoxin reductase inhibition assay data, western blot data.

REFERENCE

1. Fulda, S., Tumor Resistance to Apoptosis. *Int. J. Cancer* **2009,** *124*, 511-515.
2. Hervouet, E.; Cheray, M.; Vallette, F. M.; Cartron, P. F., DNA Methylation and Apoptosis Resistance in Cancer Cells. *Cells* **2013,** *2*, 545-573.
3. O'Gorman, D. M.; Cotter, T. G., Molecular Signals in Anti-apoptotic Survival Pathways. *Leukemia* **2001,** *15*, 21-34.
4. Pommier, Y.; Sordet, O.; Antony, S.; Hayward, R. L.; Kohn, K. W., Apoptosis Defects and Chemotherapy Resistance: Molecular Interaction Maps and Networks. *Oncogene* **2004,** *23*, 2934-2949.
5. Soengas, M. S.; Lowe, S. W., Apoptosis and Melanoma Chemoresistance. *Oncogene* **2003,** *22*, 3138-3151.
6. Paul, I.; Jones, J. M., Apoptosis Block as a Barrier to Effective Therapy in Non Small Cell Lung Cancer. *World J. Clin. Oncol.* **2014,** *5*, 588-594.
7. Krakstad, C.; Chekenya, M., Survival Signalling and Apoptosis Resistance in Glioblastomas: Opportunities for Targeted Therapeutics. *Mol. Cancer* **2010,** *9*, 135.
8. Robles, A. I.; Harris, C. C., Clinical Outcomes and Correlates of TP53 Mutations and Cancer. *Cold Spring Harb. Perspect. Biol.* **2010,** *2*, a001016.
9. Michaud, W. A.; Nichols, A. C.; Mroz, E. A.; Faquin, W. C.; Clark, J. R.; Begum, S.; Westra, W. H.; Wada, H.; Busse, P. M.; Ellisen, L. W.; Rocco, J. W., Bcl-2 Blocks Cisplatin-Induced Apoptosis and Predicts Poor Outcome Following Chemoradiation Treatment in Advanced Oropharyngeal Squamous Cell Carcinoma. *Clin Cancer Res.* **2009,** *15*, 1645-1654.
10. Silvestrini, R.; Benini, E.; Veneroni, S.; Daidone, M.; Tomasic, G.; Squicciarini, P.; Salvadori, B., p53 and *bcl-2* Expression Correlates With Clinical Outcome in a Series of Node-Positive Breast Cancer Patients. *J. Clin. Oncol.* **1996,** *14*, 1604-1610.

11. Kreuzaler, P.; Watson, C. J., Killing a Cancer: What are the Alternatives? *Nat. Rev. Cancer* **2012,** *12*, 411-424.

12. Holohan, C.; Van Schaeybroeck, S.; Longley, D. B.; Johnston, P. G., Cancer Drug Resistance: An Evolving Paradigm. *Nat. Rev. Cancer* **2013,** *13*, 714-726.

13. Kornienko, A.; Mathieu, V.; Rastogi, S. V.; Lefranc, F.; Kiss, R., Therapeutic Agents Triggering Nonapoptotic Cancer Cell Death. *J. Med. Chem.* **2013,** *56*, 4823-4839.

14. Kim, I.; Xu, W.; Reed, J. C., Cell Death and Endoplasmic Reticulum Stress: Disease Relevance and Therapeutic Opportunities. *Nat. Rev. Drug Discov.* **2008,** *7*, 1013-1030.

15. Li, X.; Zhang, K.; Li, Z., Unfolded Protein Response in Cancer: The Physician's Perspective. *J. Hematol. Oncol.* **2011,** *4* (8).

16. Yadav, R. K.; Chae, S. W.; Kim, H. R.; Chae, H. J., Endoplasmic Reticulum Stress and Cancer. *J. Cancer Prev.* **2014,** *19*, 75-88.

17. Koltai, T., Nelfinavir and Other Protease Inhibitors in Cancer: Mechanisms Involved in Anticancer Activity. *F1000Research* **2015,** *4*.

18. Bruning, A., Analysis of Nelfinavir-Induced Endoplasmic Reticulum Stress. *Methods Enzymol.* **2011,** *491*, 127-142.

19. Hamed, H. A.; Tavallai, S.; Grant, S.; Poklepovic, A.; Dent, P., Sorafenib/Regorafenib and Lapatinib Interact to Kill CNS Tumor Cells. *J. Cell Physiol.* **2015,** *230*, 131-139.

20. Fiskus, W.; Saba, N.; Shen, M.; Ghias, M.; Liu, J.; Gupta, S. D.; Chauhan, L.; Rao, R.; Gunewardena, S.; Schorno, K.; Austin, C. P.; Maddocks, K.; Byrd, J.; Melnick, A.; Huang, P.; Wiestner, A.; Bhalla, K. N., Auranofin Induces Lethal Oxidative and Endoplasmic Reticulum Stress and Exerts Potent Preclinical Activity Against Chronic Lymphocytic Leukemia. *Cancer Res.* **2014,** *74*, 2520-2532.

21. Zou, P.; Chen, M.; Ji, J.; Chen, W.; Chen, X.; Ying, S.; Zhang, J.; Zhang, Z.; Liu, Z.; Yang, S.; Liang, G., Auranofin Induces Apoptosis by ROS-Mediated ER Stress and Mitochondrial Dysfunction and Displayed Synergistic Lethality With Piperlongumine in gastric Cancer. *Oncotarget* **2015,** *6*, 36505-36521.

22. Zou, T.; Lok, C. N.; Fung, Y. M.; Che, C. M., Luminescent Organoplatinum(II) Complexes Containing Bis(N-heterocyclic carbene) Ligands Selectively Target the Endoplasmic Reticulum and Induce Potent Photo-Toxicity. *Chem. Commun.* **2013,** *49*, 5423-5425.

23. Kreutz, D.; Bileck, A.; Plessl, K.; Wolrab, D.; Groessl, M.; Keppler, B. K.; Meier, S. M.; Gerner, C., Response Profiling Using Shotgun Proteomics Enables Global Metallodrug Mechanisms of Action To Be Established. *Chem. Eur. J.* **2017,** *23*, 1881-1890.

24. Meng, X.; Leyva, M. L.; Jenny, M.; Gross, I.; Benosman, S.; Fricker, B.; Harlepp, S.; Hebraud, P.; Boos, A.; Wlosik, P.; Bischoff, P.; Sirlin, C.; Pfeffer, M.; Loeffler, J. P.; Gaiddon, C., A Ruthenium-Containing Organometallic Compound Reduces Tumor Growth Through Induction of the Endoplasmic Reticulum Stress Gene CHOP. *Cancer Res.* **2009,** *69*, 5458-5466.

25. Vidimar, V.; Meng, X.; Klajner, M.; Licona, C.; Fetzer, L.; Harlepp, S.; Hebraud, P.; Sidhoum, M.; Sirlin, C.; Loeffler, J. P.; Mellitzer, G.; Sava, G.; Pfeffer, M.; Gaiddon, C., Induction of Caspase 8 and Reactive Oxygen Species by Ruthenium-Derived Anticancer Compounds With Improved Water Solubility and Cytotoxicity. *Biochem. Pharmacol.* **2012,** *84*, 1428-1436.

26. Krysko, D. V.; Garg, A. D.; Kaczmarek, A.; Krysko, O.; Agostinis, P.; Vandenabeele, P., Immunogenic Cell Death and DAMPs in Cancer Therapy. *Nat. Rev. Cancer* **2012,** *12*, 860-875.

27. Inoue, H.; Tani, K., Multimodal Immunogenic Cancer Cell Death as a Consequence of Anticancer Cytotoxic Treatments. *Cell Death Differ.* **2014,** *21*, 39-49.

28. Iurlaro, R.; Munoz-Pinedo, C., Cell Death Induced by Endoplasmic Reticulum Stress. *FEBS J.* **2016,** *283*, 2640-2652.

29. Hoyer-Hansen, M.; Jaattela, M., Connecting Endoplasmic Reticulum Stress to Autophagy by Unfolded Protein Response and Calcium. *Cell Death Differ.* **2007,** *14*, 1576-1582.

30. Saveljeva, S.; Mc Laughlin, S. L.; Vandenabeele, P.; Samali, A.; Bertrand, M. J., Endoplasmic Reticulum Stress Induces Ligand-Independent TNFR1-Mediated Necroptosis in L929 cells. *Cell Death Dis.* **2015,** *6*, e1587.

31. Ram, B. M.; Ramakrishna, G., Endoplasmic Reticulum Vacuolation and Unfolded Protein Response Leading to Paraptosis Like Cell Death in Cyclosporine A Treated Cancer Cervix Cells is Mediated by Cyclophilin B Inhibition. *Biochim. Biophys. Acta* **2014,** *1843*, 2497-2512.

32. Chow, M. J.; Licona, C.; Wong, D. Y. Q.; Pastorin, G.; Gaiddon, C.; Ang, W. H., Discovery and Investigation of Anticancer Ruthenium-Arene Schiff-Base Complexes via Water-Promoted Combinatorial Three-Component Assembly. *J. Med. Chem.* **2014,** *57* (14), 6043-6059.

33. Chow, M. J.; Babak, M. V.; Wong, D. Y.; Pastorin, G.; Gaiddon, C.; Ang, W. H., Structural Determinants of p53-Independence in Anticancer Ruthenium-Arene Schiff-Base Complexes. *Mol. Pharm.* **2016,** *13*, 2543-2554.

34. Chow, M. J.; Licona, C.; Pastorin, G.; Mellitzer, G.; Ang, W. H.; Gaiddon, C., Structural Tuning of Organoruthenium Compounds Allows Oxidative Switch to Control ER Stress Pathways and Bypass Multidrug Resistance. *Chem. Sci* **2016,** *7*, 4117-4124.

35. *Test No. 107: Partition Coefficient (n-octanol/water): Shake Flask Method*. OECD Publishing: Paris, 1995.

36. Chantret, I.; Rodolosse, A.; Barbat, A.; Dussaulx, E.; Brot-Laroche, E.; Zweibaum, A.; Rousset, M., Differential Expression of Sucrase-isomaltase in Clones Isolated from Early and Late Passages of the Cell line Caco-2- Evidence for Glucose-Dependent Negative Regulation. *J. Cell Sci.* **1994,** *107*, 213-225.

37. Carmichael, J.; DeGraff, W. G.; Gazdar, A. F.; Minna, J. D.; Mitchell, J. B., Evaluation of a Tetrazolium-based Semiautomated Colorimetric Assay: Assessment of Chemosensitivity Testing. *Cancer Res.* **1987,** *47*, 936-942.

38. Brown, R.; Clugston, C.; Burns, P.; Edlin, A.; Vasey, P.; Vojtesek, B.; Kaye, S. B., Increased Accumulation of p53 Protein in Cisplatin-Resistant Ovarian Cell Lines. *Int. J. Cancer* **1993,** *55*, 678-684.

39. Roy, G.; Horton, J. K.; Roy, R.; Denning, T.; Mitra, S.; Boldogh, I., Acquired Alkylating Drug Resistanc of a Human Ovarian Carcinoma Cell Line is Unaffected by Altered Levels of Pro- and Anti-Apoptotic Proteins. *Oncogene* **2000,** *19*, 141-150.

40. Boyer, J.; McLean, E. G.; Aroori, S.; Wilson, P.; McCulla, A.; Carey, P. D.; Longley, D. B.; Johnston, P. G., Characterization of p53 Wild-Type and Null Isogenic Colorectal Cancer Cell Lines Resistant to 5-Fluorouracil, Oxaliplatin, and Irinotecan. *Clin. Cancer Res.* **2004,** *10*, 2158-2167.

41. Violette, S.; Poulain, L.; Dussaulx, E.; Pepin, D.; Faussat, A. M.; Chambaz, J.; Lacorte, J. M.; Staedel, C.; Lesuffleur, T., Resistance of Colon Cancer Cells to Long-term 5-fluorouracil Exposure is Correlated to the Relative Level of Bcl-2 and Bcl-X(L) in Addition to Bax and p53 Status. *Int. J. Cancer* **2002,** *98*, 498-504.

42. Macleod, K. F.; Sherry, N.; Hannon, G.; Beach, D.; Tokino, T.; Kinzler, K.; Vogelstein, B.; Jacks, T., p53-Dependent and Independent Expression of p21 During Cell Growth, Differentiation, and DNA Damage. *Genes Dev.* **1995,** *9*, 935-944.

43. Jungwirth, U.; Kowol, C. R.; Keppler, B. K.; Hartinger, C. G.; Berger, W.; Heffeter, P., Anticancer Activity of Metal Complexes: Involvement of Redox Processes. *Antioxid. Redox. Signal.* **2011,** *15*, 1085-1127.

44. Bragadin, M.; Scutari, G.; Folda, A.; Bindoli, A.; Rigobello, M. P., Effect of Metal Complexes on Thioredoxin Reductase and the Regulation of Mitochondrial Permeability Conditions. *Ann. N. Y. Acad. Sci.* **2004,** *1030*, 348-354.

45. Zou, T.; Lum, C. T.; Lok, C. N.; Zhang, J. J.; Che, C. M., Chemical Biology of Anticancer Gold(III) and Gold(I) Gomplexes. *Chem. Soc. Rev.* **2015,** *44*, 8786-8801.

46. Witte, A. B.; Anestal, K.; Jerremalm, E.; Ehrsson, H.; Arner, E. S., Inhibition of Thioredoxin Reductase but Not of Glutathione Reductase by the Major Classes of Alkylating and Platinum-Containing Anticancer Compounds. *Free. Radic. Biol. Med.* **2005,** *39*, 696-703.

47. Hetz, C., The Unfolded Protein Response: Controlling Cell Fate Decisions Under ER stress and Beyond. *Nat. Rev. Mol. Cell Biol.* **2012,** *13*, 89-102.

48. Ron, D.; Walter, P., Signal Integration in the Endoplasmic Reticulum Unfolded Protein Response. *Nat. Rev. Mol. Cell Biol.* **2007,** *8*, 519-529.

49. Oyadomari, S.; Mori, M., Roles of CHOP(GADD153) in Endoplasmic Reticulum Stress. *Cell Death Differ.* **2004,** *11*, 381-389.

FOR TABLE OF CONTENT USE ONLY

Induction of the Endoplasmic Reticulum Stress Pathway by Highly Cytotoxic Organoruthenium Schiff-Base Complexes

Mun Juinn Chow,[1] Maria V. Babak,[2] Kwan Wei Tan,[3] Mei Chi Cheong,[3] Giorgia Pastorin[2,4], Christian Gaiddon[5, 6] and Wee Han Ang*[3, 4]*